Toxicology Research

PAPER

View Article Online
View Journal | View Issue

Cite this: *Toxicol. Res.*, 2018, **7**, 244

Mechanistic insight into ROS and neutral lipid alteration induced toxicity in the human model with fins (Danio rerio) by industrially synthesized titanium dioxide nanoparticles†

Suresh K. Verma,[a] Ealisha Jha,[b] Pritam Kumar Panda,[a] Mohana Mukherjee,[a] Arun Thirumurugan,[c] Hardik Makkar,[d] Biswadeep Das,[a] S. K. S. Parashar[e] and Mrutyunjay Suar*[a]

Received 6th November 2017,
Accepted 16th January 2018

DOI: 10.1039/c7tx00300e

rsc.li/toxicology-research

The toxicological impact of TiO_2 nanoparticles on the environment and human health has been extensively studied in the last few decades, but the mechanistic details were unknown. In this study, we evaluated the impact of industrially prepared TiO_2 nanoparticles on the biological system using zebrafish embryo as an *in vivo* model. The industrial synthesis of TiO_2 nanoparticles was mimicked on the lab scale using the high energy ball milling (HEBM) method by milling bulk TiO_2 particles for 5 h, 10 h, and 15 h in an ambient environment. The physiochemical properties were characterized by standard methods like field emission scanning electron microscopy (FESEM), dynamic light scattering (DLS), X-ray diffraction (XRD) and UV-Visible spectroscopy. *In vivo* cytotoxicity was assessed on zebrafish embryos by the evaluation of their mortality rate and hatching rate. Experimental and computational analysis of reactive oxygen species (ROS) induction, apoptosis, and neutral lipid alteration was done to study the effects on the cellular level of zebrafish larvae. The analysis depicted the change in size and surface charge of TiO_2 nanoparticles with respect to the increase in milling time. *In silico* investigations revealed the significant role of ROS quenching and altered neutral lipid accumulation functionalised by the molecular interaction of respective metabolic proteins in the cytotoxicity of TiO_2 nanoparticles with zebrafish embryos. The results reveal the hidden effect of industrially synthesized TiO_2 nanoparticle exposure on the alteration of lipid accumulation and ROS in developing zebrafish embryos. Moreover, the assessment provided a detailed mechanistic analysis of *in vivo* cytotoxicity at the molecular level.

Introduction

Recent advances in nanotechnology has led to the exploration of numerous applications of metal oxide nanoparticles in day to day life. Metal oxide nanoparticles like ZnO,[1,2] CuO and TiO_2 have gained a lot of popularity because of their peculiar properties and immense potential in different applications.[3] Among these, TiO_2 nanoparticles are the most studied and industrially utilised. Their multiple applications include their use as additives in sunscreen products, printing ink, cement, rubber, paints, paper, sugar, toothpaste, film, implanted biomaterials, bio-medical ceramics, antimicrobial plastic packaging and self-cleaning sanitary ceramics.[4–6] The versatility in the usage of TiO_2 nanoparticles in these applications is due to their peculiar properties such as good fatigue strength, resistance to corrosion, durability, biocompatibility, whitening, photocatalysis, electrical characteristics, and excellent optical performance.[7–11] To meet the extensive demand for TiO_2 nanoparticles due to these multiple applications, researchers and industries have explored different methods to synthesize TiO_2 nanoparticles on both the lab and industrial scale. Some of these include chemical synthesis,[12] biological synthesis[13] and physical synthesis[14] processes. Although chemical and biological synthesis processes have provided applicative solutions for the synthesis of TiO_2 nanoparticles, there are limitations to the bulk synthesis. Moreover, purity concerns exist due to the use of chemicals and biomolecules. Physical synthesis pro-

[a]*School of Biotechnology, KIIT University, Bhubaneswar, Orissa, 751024, India. E-mail: msbiotek@yahoo.com, msuar@kiitbiotech.ac.in*
[b]*Memorial University of Newfoundland, Department of Physics and Physical Oceanography, St John's, Newfoundland and Labrador, NL A1C 5S7, Canada*
[c]*Advanced Materials Laboratory, Department of Mechanical Engineering, Faculty of Mathematical and Physical Sciences, University of Chile, Santiago, Chile*
[d]*KIIT Technology Business incubator, KIIT University, Bhubaneswar, Orissa, 751024, India*
[e]*School of Applied Sciences, KIIT University, Bhubaneswar, Orissa, 751024, India*
†Electronic supplementary information (ESI) available. See DOI: 10.1039/c7tx00300e

cesses like mechanical milling have provided a potential solution to these problems. A commonly used physical milling process for nanoparticles synthesis is generally referred as the "high energy ball milling technique (HEBM)". HEBM has been recognized for the synthesis of nanoparticles without any complexity.[15–18] The benefits of HEBM over other reported physical and chemical methods have been the simplicity, reliability, and reproducibility.[19] Moreover, it can be recognized as a "green methodology" due to the avoidance of any harmful chemicals, and compatibility towards the ecosystem. Due to these beneficial parameters, with no compromise in quality, HEBM has been used by industries for the production of TiO_2 nanoparticles on a large scale.

With the extensive surge in the usage of TiO_2 nanoparticles, their exposure to biotic and abiotic factors of the ecosystem has also increased. Along with the direct exposure to the human body by related products, indirect exposure has also increased with consumption of water containing industrial effluents and human daily life discharges. The continuous discharge and accumulation in water bodies have raised concerns over the nanotoxicity of TiO_2 nanoparticles to human health as well as to the fitness of aquatic organisms.[20] Exposure to TiO_2 nanoparticles up to concentration ranges of 10 mg L^{-1} and 1 g L^{-1} has been reported to be toxic for aquatic organisms like rainbow trout[21] and zebrafish.[22] Studies have been done to report *in vitro*[23] and *in vivo* toxicological assessments of TiO_2 nanoparticles on different biological models.[20,21,24] *In vitro* studies using different cell line models have revealed the cytotoxic nature of TiO_2 nanoparticles due to the generation of ROS, lipid peroxidation and disturbance in the physiological processes of live models. Moreover, different pathological outcomes of toxicity in biological systems on exposure to TiO_2 nanoparticles including inflammation, apoptosis, fibrosis, hypertrophy, metaplasia and carcinogenesis have been reported.[25] Various factors that have been recognized as a result of the cytotoxic effects of nanoparticles include (1) internalization into cells,[26,27] (2) production of reactive oxygen species (ROS),[28,29] (3) DNA damage,[30] and (4) lipid peroxidation.[31] Gurr *et al.*[32] and the Long group[33] have recently reported ROS production and cell damage in human bronchial epithelial cells and brain microglia exposed to TiO_2 nanoparticles. A number of groups have also reported that the size and shape of the nanoparticles are important factors for their cytotoxic effects.[34,35] The charge of the nanoparticles has also been found to play an important role in deciding the extent of their cytotoxicity.[36] These reports have sketched various mechanisms of toxicity, however, a detailed analysis on the molecular level is still needed. Moreover, these studies have provided information about the toxicity of TiO_2 nanoparticles that are either prepared on a lab scale by the different chemical processes,[37] or have been directly purchased from the commercial market with an unknown route of preparation. There is a gap in information about the *in vivo* and *in vitro* cytotoxic effects of industrially prepared TiO_2 nanoparticles, therefore the described reports are debatable regarding real-world exposure. Based on these facts, detailed mechanistic studies of the cytotoxic effects of industrially synthesized TiO_2 nanoparticles on the aquatic ecosystem as well as human systems are needed. With this study, we have tried to fill that gap by assessing the *in vivo* cytotoxicity of industrially prepared TiO_2 nanoparticles on the zebrafish model, for the first time. TiO_2 nanoparticles were prepared by the HEBM technique as a prototype for industrial-scale synthesis and the *in vivo* cytotoxicity caused by them was investigated to show their impact in a real case.

Although *in vitro* studies on the toxicity of the nanoparticles in mammalian cell lines have been considered as a standard means for risk prediction in human beings, traditional *in vivo* tests are time-consuming, expensive and require a large amount of particles. Moreover, the cell-based assay is limited in mirroring the whole animal body metabolism.[38] Using zebrafish and their embryos as the model for *in vivo* studies is attractive to researchers since this model overcomes the limitations of traditional mammalian cell lines and mouse models. They have been used in vertebral genetics, developmental biology and toxicological research because of their high degree of genetic and physiological similarities to mammals. Moreover, they have been recognized as a popular model for the toxicological assessment of environment pollutants.[39] Recently, many reports have been made on the *in vivo* toxicological assessment of different nanoparticles like silver, zinc oxide, gold and TiO_2 using the zebrafish model.[40,41] In particular, various kinds of toxicological studies have been reported with respect to TiO_2 nanoparticles. Wang *et al.*[42] and Bar-Ilan *et al.*[43] have recently described the pathological outcomes of exposure of TiO_2 nanoparticles to the retinal tissues and other tissues at different concentrations. Moreover, the studies have been expanded to the include the molecular aspects of the toxicological effects on aquatic bodies induced by TiO_2 nanoparticles alone and in combination with other particles.[44] However, the toxicity studies of commonly utilized industrially prepared nanoparticles along with the toxicological effects at the core molecular level with mechanistic details are yet to be reported.

In this study, we have evaluated the *in vivo* toxicity of industrially prepared TiO_2 nanoparticles on the zebrafish embryo model, assessing their developmental and cytological effects. Studies of ROS generation, apoptosis evaluation, and effects on neutral lipid accumulation changes were done to determine the mechanism of toxicity both experimentally and computationally. The findings are discussed with reference to previous reports, experimental data and the observed insights of industrially prepared TiO_2 nanoparticles mimicked at the lab scale using the HEBM technique. The studies depict the dose-dependent toxicological behavior of TiO_2 nanoparticles as a consequence of ROS variation, enhanced apoptosis and neutral lipid accumulation in the zebrafish embryo.

Materials and methods

Materials

Bulk TiO_2 (~110 nm) was purchased from Merck for synthesis of the nanoparticles. Tungsten carbide balls and container

were obtained from Retsch. All the chemicals used for making HF buffer were of analytical grade and purchased from Merck. All the buffers were prepared in deionised water.

Synthesis of TiO_2 nanoparticles

Synthesis of TiO_2 nanoparticles was performed by milling bulk TiO_2 particles. High energy ball milling (Retsch, PM400) was performed in the tungsten carbide (WC) container (250 mL) using WC balls (10 mm) at 300 rpm with the ball to powder ratio of 20 : 1 in toluene medium. Milling was done for 15 h and the synthesized nanoparticles were collected at 5 h, 10 h and 15 h milling time for biological experiments. For cytotoxicity evaluation, nanoparticle suspensions were prepared in Holtfreter medium (HF)[45] by sonication at an amplitude of 50 for 5 minutes with no pulse.

Characterization of TiO_2 nanoparticles

The synthesized TiO_2 nanoparticles were characterized for their physiochemical properties by standard available techniques. Size was determined by FESEM (Zeiss, Model EVO 60) equipped with an Oxford Inca energy dispersive X-ray spectrometer (EDS), while hydrodynamic size in HF medium suspension was determined by a Zetasizer (Malvern, Zetasizer, Nano ZS). Zeta potential was measured by the dynamic light scattering technique using a Zetasizer (Nano ZS, Malvern, UK). Optical properties were determined by observing UV-Visible spectra, measuring the spectrum of the suspension in the range of 200 nm–800 nm in a UV-Vis NIR spectrophotometer (Cary 60, Agilent). Band gap energy was calculated according to the literature[46] and presented as a histogram for the different nanoparticles. Structural analysis was performed by X-ray diffraction technique using an X-ray diffractometer (X-PERT-PRO, Pan Analytical) with CuKα radiation (λ = 0.15418 nm) over the range of angles from 25° to 80°. XRD analysis of samples was conducted in powder mode.

Zebrafish maintenance and egg production

Zebrafish maintenance was carried out in a fish maintaining system supplied by Aquaneering (San Diego, USA). The water parameters were as follows: temperature: 27 ± 0.5 °C, conductivity: 744 μs, hardness: 379 mg L^{-1} $CaCO_3$ (21.30 dH), pH: 7.5 ± 0.25, dissolved oxygen: 10.5 ± 0.5 mg L^{-1} O_2 (95% saturation) and 12 : 12 dark : light photoperiod. Fishes were fed with dried bloodworms available in the market. The breeding setup was in a breeding tank, supplied by Aquaneering, in fish water with 2 : 3 male : female ratio. Embryos obtained were reared in Holtfreter medium (HF). For cytotoxicity assays, embryos were exposed to the HF medium containing TiO_2 nanoparticles.

Embryo and larvae cytotoxicity assays

Cytotoxicity assays were performed with embryos at 3–3.5 hours post fertilization (hpf) at the blastula stage. Toxicity assays were conducted according to the protocol mentioned by Vaughan *et al.*[47] Exposure of embryos was done in the concentration range of 10–250 μg mL^{-1} of bulk and TiO_2 nanoparticles in HF buffer for 96 h in a 24 well plate. The photoperiod was maintained for the experimental set up with light/dark exposure of 12 h/12 h at 27 ± 0.5 °C. The number of embryos was kept at 20 for each set of experiments. Untreated embryos were taken as the control. The hatching percentage was determined as the number of embryos hatched by 48 h and 96 h post fertilization as compared to the untreated group. Viability percentage was expressed as the number of live embryos after 96 h post fertilization as compared to the untreated group. For morphological change analysis, direct observation was done with the help of a stereomicroscope. All the experiments were performed in triplicate. The study was approved by the Institutional Animal Ethics Committee of KIIT University and all protocols were done as per the approval of the relevant guidelines of IAEC of KIIT University.

Cellular ROS analysis in embryonic zebrafish

To determine the mechanism of cytotoxicity induced by the synthesized TiO_2 nanoparticles, the analysis of cellular oxidative stress was done by measuring the fluorescence intensity of reactive oxygen species (ROS) stained by ROS permanent dye 2,7-dichlorodihydrofluorescein diacetate (H_2DCFDA) (Invitrogen, ThermoScientific) using flow cytometry.[48] Untreated and TiO_2 nanoparticles treated (50 μg mL^{-1} and 250 μg mL^{-1}) 72 h hatched embryos were sacrificed by incubating them in ice for 30 min and a single cell suspension was prepared by sonication. Cell suspensions were then stained with 1.25 mg L^{-1} of H_2DCFDA and incubated in the dark at room temperature. Following incubation, the samples were washed to remove extra stains, and were kept on ice for flow cytometry analysis. Cells were analyzed by flow cytometry using an Attune focusing slow cytometer (ThermoScientific, USA) equipped with a 488 nm argon laser. The data were analyzed in facsxpress 5 (Denovo, CA) and presented as a histogram.

Neutral lipid analysis in embryonic zebrafish

To analyze neutral lipid alteration induced in embryonic zebrafish by TiO_2 nanoparticles exposure, fluorescence microscopy was performed to stain triggered neutral lipids with the help of the neutral lipid stain LipidTOX™ (Invitrogen, ThermoScientific). Untreated and TiO_2 nanoparticles treated (50 μg mL^{-1} and 250 μg mL^{-1}) zebrafish embryos were washed thrice with sterilized HF buffer to remove extra attached particles. Following the washing, they were stained with 2 mg L^{-1} of stain and incubated for 20 min in the dark. The extra stain was then removed by washing. Observations were made using the red filter of the microscope (EVOS, ThermoScientific) and images were taken.

Acridine orange staining for apoptosis analysis

Apoptosis was induced in embryonic zebrafish exposed to synthesized TiO_2 nanoparticles with the help of the acridine orange staining protocol mentioned by Deng *et al.*[49] In brief, untreated and TiO_2 nanoparticle treated (50 μg mL^{-1} and 250 μg mL^{-1}) zebrafish embryos were washed two times with HF buffer after treatment and stained with 5 μg mL^{-1} AO dis-

solved in HF buffer for 20 min. Following the staining, the embryos were washed with sterilized HF buffer to remove the extra stain and were observed in the green channel of the fluorescence microscope (EVOS, ThermoScientific).

In silico molecular docking for TiO_2 interaction

Molecular docking studies were used to determine the interaction of the ligand and the protein to know the preferred binding orientations of ligand that conferred a minimum binding energy (generally in negative energies).[50] In this study, molecular docking analysis was carried out with the help of Autodock 4.2 [51] using TiO_2 as ligand and he1a, sod1, tp53 as receptor proteins. The structure of TiO_2 was drawn using Chimera[52] and its geometry was optimised using the Gaussian 03 program. The receptor proteins were subjected to energy minimization using the Chimera program. The parameters for "Ti" were set for Autodock 4.2. Grid dimensions were set to 40 × 40 × 40, with a spacing of 1 Å for all the protein receptors. For grid dimensions, Lamarckian genetic algorithms (LGA) were used. A genetic algorithm was used for docking runs using a population size of 150 with the maximum number of evaluations set to 2 500 000 and maximal generations. The post docking analysis was performed using Autodock 4.2 analysis tools, using conformational clustering, which was visualized using the Chimera and Discovery Studio Visualizer. 2D interaction plots were derived from the receptor complexes having TiO_2 as a ligand by using LigPlot+.[53] Protein–protein interaction of MTTP and apoa1a were done using HEX8.0.[54]

Results

Physiochemical characterization of synthesized TiO_2 nanoparticles

In order to evaluate the toxicity of industrially synthesized TiO_2 nanoparticles, the industrial synthesis of TiO_2 nanoparticles was mimicked at the lab scale using the high energy ball milling technique (HEBM). As shown in Fig. 1A, B, C, D, the size of TiO_2 nanoparticles determined by FESEM was reduced, with an increase in milling time, to 85 ± 10 nm from 110 ± 09 nm of bulk TiO_2 nanoparticles after 5 h of milling. On further milling for 10 h and 15 h, the size decreased to 62 ± 14 nm and 46 ± 16 nm, respectively (Table 1). Fig. S1(a)† shows the reduction of the hydrodynamic size of nanoparticles in HF medium as determined by dynamic light scattering. The hydrodynamic diameter was also reduced to 461.2 ± 32 nm, 326.6 ± 18 nm and 276.5 ± 21 nm after 5 h, 10 h and 15 h of milling, respectively, from 514.4 ± 24 nm of bulk particles in HF medium (Table 1). To determine the stability and agglomeration tendency of synthesized TiO_2 nanoparticles in HF medium, their zeta potentials were measured using the Zetasizer. Fig. S1(b)† shows the zeta potentials of bulk, 5 h, 10 h and 15 h milled TiO_2 nanoparticles in HF medium. The zeta potential increased with the milling time. In comparison to the zeta potential of −34.2 ± 6.3 mV for bulk TiO_2 particles, after 5 h, 10 h and 15 h of milling, the TiO_2 nanoparticles exhibited increasing zeta potentials of −28.6 ± 4.2 mV, −24.3 ± 3.6 mV and −16.7 ± 7.4 mV, respectively (Table 1). Optical properties were determined by UV-Visible spectroscopy. Band gap energy was also calculated as per the literature[46] report to confirm the change in the size of the synthesized TiO_2 nanoparticles. Fig. S1(c)† shows the blue shift in the absorption peak with the increase in the milling time of the TiO_2 particles. On calculating the band gap energy (Fig. S1(d)†), the 15 h milled nanoparticles were found to have the highest band gap (4.6 eV) in comparison to the 10 h and 5 h milled nanoparticles and bulk particles, which were 4.2 eV, 3.8 eV and 3.4 eV (Table 1), respectively, and were statistically significant. The increase in band gap energy can be attributed to the induced localized gap states in Ti.[8–10] Moreover, the increased oxygen vacancies can be due to the increased band gap with increase in milling time.[10,11] XRD patterns were obtained for all four types of nanoparticles as shown in Fig. 1E. The peaks of the nanoparticles were identified, corresponding to (101), (004), (200), (105), (211), (204), (116), (220), and (215) crystal planes. All diffraction peaks were well defined and can be perfectly assigned to the anatase TiO_2 (JCPDS-21-1272).[8,55] The broadening of the peak depicted the decreasing size of the nanoparticles with increase in milling time.

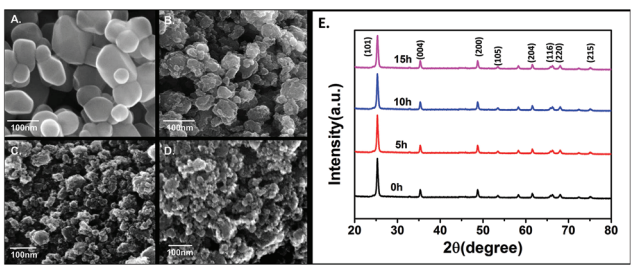

Fig. 1 Characterization of bulk, 5 h, 10 h and 15 h milled TiO_2 nanoparticles prepared by the HEBM method. FESEM images of (A) bulk, (B) 5 h nano TiO_2 (C) 10 h nano TiO_2 (D) 15 h nanoTiO_2. (E) XRD spectra of nanoparticles.

Interaction of TiO_2 nanoparticles with zebrafish embryo

Toxicological effects of bulk TiO_2 and nanoparticles were investigated by determining the different physiological parameters like viability percentage, hatching percentage, morphological phenotypic alteration in tail flexion and notochord malformation[56] of zebrafish embryo exposed to a concentration range of 10–250 μg mL^{-1}. For detailed analysis, lower (50 μg mL^{-1}) and higher (250 μg mL^{-1}) concentrations of bulk TiO_2 and nanoparticles were chosen to determine their uptake and respective effects on the hatching rate and viability rate of embryos exposed for 24 h to 96 h. As shown in Fig. S2,† the survival percentage in the control solvent was greater than 90%, which was significantly reduced in embryos exposed to the 5 h, 10 h and 15 h milled TiO_2 nanoparticles with an increase in concentration. There was no significant reduction in the survival of embryos exposed to 10 μg mL^{-1} of bulk particles for 24 h; however, it was substantial at 72 h and 96 h exposure. A similar trend was found in the case of the hatching

Table 1 Physiochemical characterization of the nanoparticles; the table shows the sizes determined by FESEM, hydrodynamic diameter and zeta potential of TiO_2 nanoparticles in different media. Band gap was determined by the SPR peak of the UV-Visible spectrum

Nanoparticles	Size (nm) by FESEM	Hydrodynamic diameter (nm)		Zeta potential (mV)		Band gap (eV)
		Aq.	HF	Aq.	HF	
Bulk TiO_2 particles	110 ± 09	268.2 ± 68	514.4 ± 24	−46.6 ± 7.7	−34.2 ± 6.3	3.4
5 h TiO_2 nanoparticles	85 ± 10	239.2 ± 29	461.2 ± 32	−38.2 ± 7.1	−28.6 ± 4.2	3.8
10 h TiO_2 nanoparticles	62 ± 14	185.5 ± 28	326.6 ± 18	−26.4 ± 6.8	−24.3 ± 3.6	4.2
15 h TiO_2 nanoparticles	46 ± 16	132.4 ± 20	276.5 ± 21	−21.2 ± 6.6	−16.7 ± 7.4	4.6

percentage (Fig. S3†). It was found that the hatching percentage of embryos was about 20% at 48 hpf in the control solvent, which was further significantly reduced with exposure to increased concentrations of TiO_2 nanoparticles. The trends were similar at 96 hpf, with the greatest reduction to 38% in the case of exposure to 15 h TiO_2 nanoparticles as compared to >90% hatching in the control solvent. The hatching and viability percentage were further reduced with the increase in milling time of the TiO_2 nanoparticles. With the information obtained from these experimental observations, a concise and comparative study was done with exposure to 50 μg mL^{-1} and 250 μg mL^{-1} as the lower and higher concentration, respectively. As shown in Fig. 2A and B, the hatching percentage was decreased to 87 ± 2% (mean ± SD), 80 ± 5%, 76 ± 3% and 60 ± 4% with exposure for 96 h to the bulk and TiO_2 nanoparticles milled for 5 h, 10 h and 15 h at lower concentration, in comparison to 95 ± 2% in the control solvent. There was further decrease to 72 ± 2%, 60 ± 4%, 45 ± 2% and 38 ± 3% on exposure to the bulk and TiO_2 nanoparticles milled for 5 h, 10 h and 15 h, respectively, at concentration of 250 μg mL^{-1}, as compared to 90 ± 2% in the control solvent. The reduction was also dependent on exposure time. Along with this, the percentage survivability of zebrafish embryos exposed to bulk TiO_2 and nanoparticles showed the same trend (Fig. 2C and D); it was also found to decline with exposure time. The survivability of embryos in the control solvent was >90% till 96 h exposure. At higher concentration, there was a decrease to 46 ± 4%, 36 ± 2%, 32 ± 4% and 28 ± 4% on exposure to the bulk, and TiO_2 nanoparticles milled for 5 h, 10 h and 15 h, respectively. This decline was also dependent on the milling time of TiO_2 particles. These observations suggest that the toxicological behavior of bulk and nano TiO_2 particles is size and exposure time dependent. Fig. S4† shows the uptake of TiO_2 nanoparticles as analyzed by the granularity difference shown by the mean side scatter of the flow cytometry data.[57] Uptake of nanoparticles was found to be increased with the increase in milling time. The results were well supported by analysis of bright field images taken to observe the phenotypic malformation. As shown in Fig. 3, bulk TiO_2 particles were found to be accumulated at the chorion surface of 48 hpf embryos with induction of tail bending at higher concentration. The effects were seen more in embryos exposed to TiO_2 nanoparticles milled for 5 h, 10 h, and 15 h. Embryos exposed to TiO_2 nanoparticles milled for 5 h showed abnormalities such as having unusual notochord development and loss of normal chorion shape. Moreover, the bending of the tail was also observed at exposure to higher concentration. The deformities in phenotype and development were clearly visible in the embryos exposed to TiO_2 nanoparticles milled for 10 h and 15 h, which had abnormal yolk sac and the loss of chorion.

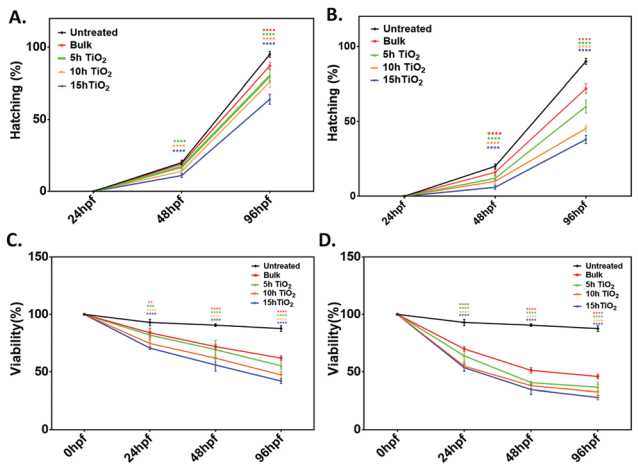

Fig. 2 Graphical representation of hatching rate and viability rate of zebrafish embryo treated with low (50 μg mL^{-1}) and high (250 μg mL^{-1}) concentrations of bulk TiO_2 and nanoparticles. (a), (b) The hatching rate at low and high concentration, respectively; (c), (d) the viability percentage at low and high concentration, respectively. Percentages were determined for a group of 20 embryos. The values represent the mean ± SD of three independent experiments. *P < 0.05 denotes the significant change from untreated control, bulk and 7 h exposed embryos as obtained from two way ANOVA analysis; * represents the degree of significance.

In silico analysis of TiO_2 nanoparticles interaction

For a better understanding of the interaction of TiO_2 nanoparticles with zebrafish embryos, and their effects on hatching, the *in silico* approach was taken. Molecular docking analysis of hatching enzyme (he1a)[58] with TiO_2 nanoparticles showed hydrophobic and hydrogen bonding interactions with different amino acid residues. As shown in Fig. 4A, Autodock predicted the hydrophobic interaction of TiO_2 nanoparticles with threonine (Thr), cysteine (Cys), isoleucine (Ile), and tyrosine (Tyr) residues. Interaction *via* hydrogen bond was predicted with the asparagine (Asn) residue. Ligplot presentation showed the

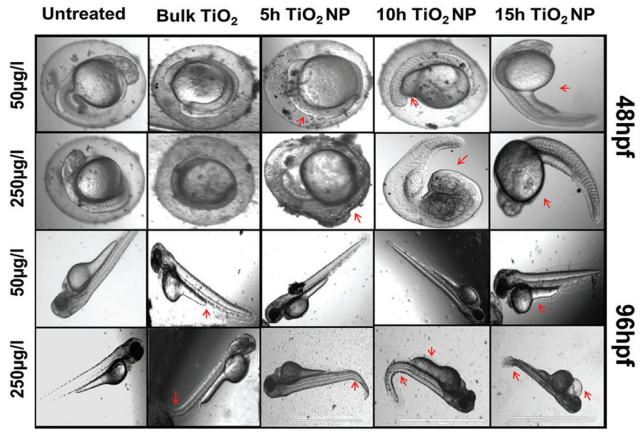

Fig. 3 Morphological and anatomical changes in zebrafish embryo treated with low (50 μg mL^{-1}) and high (250 μg mL^{-1}) concentrations of bulk TiO_2 and nanoparticles. The bright field image was taken after washing twice with HF buffer. The red arrows indicate the deformation in embryos (deformation in chorion and yolk sac in 48 hpf, and deformation in the tail, notochord and heart development in 96 hpf). Scale bar represents 1000 nm.

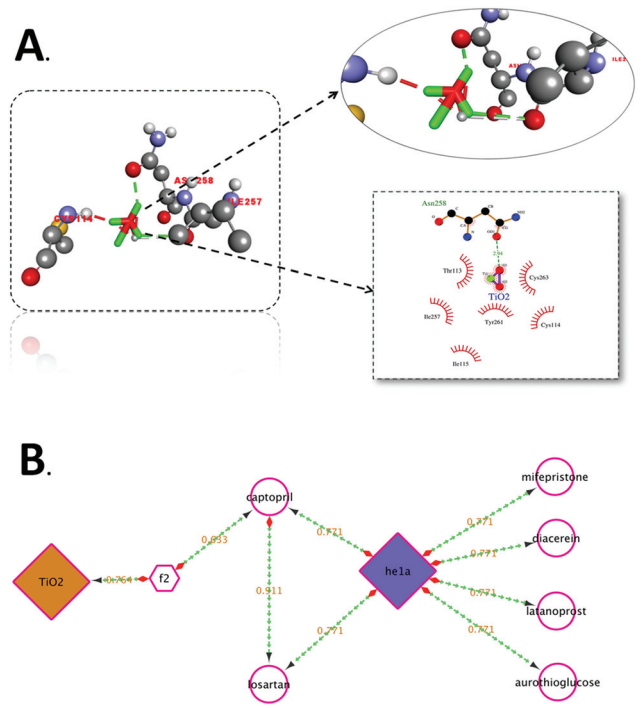

Fig. 4 A. Molecular interaction of he1a protein with TiO_2, visualized using Discovery Studio Visualizer, showing the mode of interaction with residues. B. Pathway showing the TiO_2 interaction mechanism through f2 catalyst to he1a.

H-bond length of 2.94 Å. Pathway investigation through STITCH[59] indicated the interaction of TiO_2 with he1a by means of the f2 catalyst (thrombin) and captopril (inhibitor) with a useful score of 0.764, 0.633 and 0.771, individually. Some other enzymes were also found to be linked to the

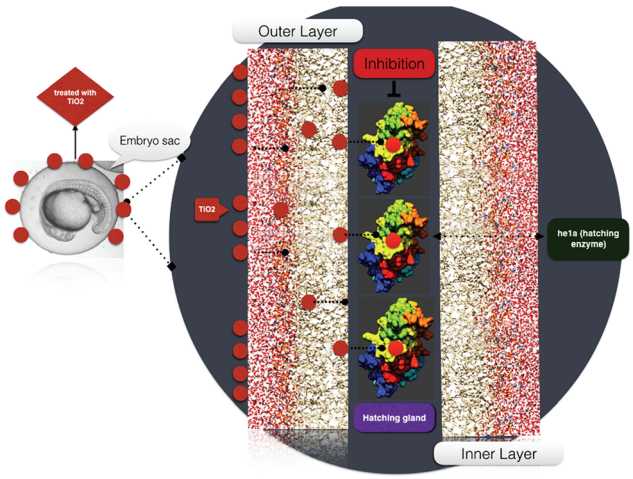

Fig. 5 Schematic representation of the effect of TiO_2 nanoparticles on zebrafish embryo hatching.

pathway as shown in Fig. 4B. With the relevance of *in silico* and experimental data, the interaction and effect on hatching were shown by schematic diagram (Fig. 5).

Analysis of the cellular cytotoxicity of bulk TiO_2 and nanoparticles

The determination of the cytotoxic effects of bulk TiO_2 and nanoparticles to embryonic zebrafish at the cellular level was done by assessment of oxidative stress, steatosis and apoptosis with experimental (*in vivo*) and computational (*in silico*) approaches.

Oxidative stress analysis

As shown in Fig. 6(A) and (B), the flow cytometric determination of oxidative stress by measuring the fluorescence of DCFDA displayed the exposure and milling time dependent ROS scavenging effect of bulk and TiO_2 nanoparticles in zebrafish embryos. Bulk TiO_2 particles were found to induce enhanced ROS generation while 5 h, 10 h and 15 h milled nanoparticles showed ROS quenching at both low and high concentrations. *In silico* analysis was performed to understand the molecular level interaction of TiO_2 nanoparticles with the ROS inducing gene sod1.[60] Docking predictions showed 9 conformations with H-bonds. The best conformation with H-bond of minimum free energy was predicted with phenylalanine (Phe) and alanine (Ala) residues of sod1 with bond lengths of 3.06 Å, 2.79 Å and 2.62 Å, respectively, as shown in Fig. 6(C) and Table 2.

Steatosis analysis

Steatosis effects in embryonic zebrafish exposed to TiO_2 nanoparticles were determined by the analysis of alterations in neutral lipids. Fig. 7 shows the intensity of LipidTOX™ stained neutral lipid in the head and tail regions of untreated and TiO_2 nanoparticle treated embryonic zebrafish. Size and concentration dependent enhanced accumulation of neutral lipid

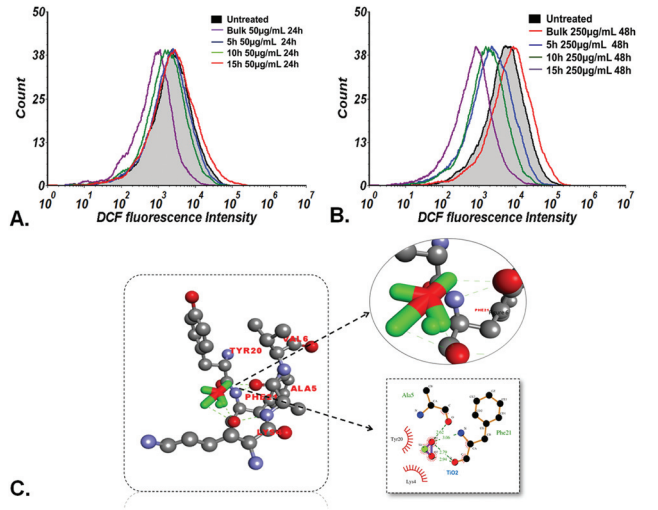

Fig. 6 Oxidative stress analysis; ROS measurement of zebrafish embryos treated for 24 h and 48 h at low (50 mg L^{-1}) and high (250 mg L^{-1}) concentrations of bulk TiO_2 and nanoparticles as determined by flow cytometry. Fluorescence intensity of cells shifted towards the left at (A) 48 hpf and (B) 96 hpf in accordance with the milling time. (C) Molecular docking analyses of sod1 with TiO_2 nanoparticles showing interacting residues using LigPlot+ and Discovery Studio Visualizer.

Table 2 Binding affinities of TiO_2 with different protein receptors, showing H-bonding interactions

Receptors	Binding energy (kcal mol^{-1})	Binding residues	H-Bond length	Atoms involved (TiO_2-receptor residues)
he1a	−3.39	Asn258	2.94	O1–OD1
sod1	−3.80	Val82	2.96	O2–N
		Asn66	2.38	O1–OD1
		Asn66	3.12	O2–OD1
apoa1a	−2.44	Leu84	2.73	O1–O
		Leu84	3.07	O2–O
		Thr85	2.89	O1O
tp53	−3.14	Arg314	2.80	O2–N
		Arg310	3.07	O2–O
		Arg310	3.14	O1–O
		Glu313	3.10	O1–OE1
		Glu302	2.96	O1–OE1

was found in the zebrafish larvae head, notochord, and tail region treated with bulk TiO_2 and 5 h, 10 h and 15 h milled nanoparticles. For a better understanding of the phenomenon, a computational approach was taken. Molecular docking analysis of apoa1a[61] (apolipoprotein) with TiO_2 predicted direct interaction *via* H-bonding with leucine (Leu) and threonine (Thr) residues, with lengths of 3.07 Å, 2.73 Å and 2.89 Å, respectively, as shown in Fig. 8(A) and Table 2. Since neutral lipids synthesized by apolipoprotein have been reported to be carried by carrier proteins (MTTP),[62] the interaction of MTTP with apoa1a was also analyzed by HEX docking (Fig. 8B). As predicted by HEX, apoa1a was directly interacting with MTTP at three different cluster regions with strong H-bonding, having a total binding energy of −576.01 kcal mol^{-1}. The interaction indicated the direct influence of apoa1a on the function of MTTP.

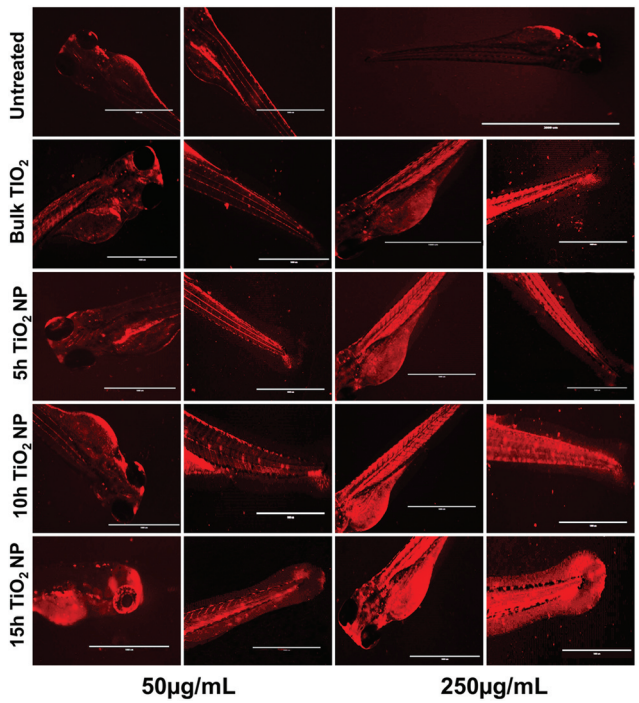

Fig. 7 Fluorescent images of zebrafish larvae stained with Lipidtox dye treated with TiO_2 nanoparticles at concentrations of 50 µg mL^{-1} and 250 µg mL^{-1}, presenting alterations in neutral lipids in different tissues. Neutral lipid accumulation alteration was found to vary with the size and concentration of the nanoparticles.

Apoptosis analysis

With reference to the physiological studies done so far in this report, better understanding with mechanistic insight for the outcome of the TiO_2 nanotoxicity was accomplished by assessing apoptosis in TiO_2 exposed embryonic zebrafish. As shown in Fig. 9, acridine orange staining showed enhanced green patches depicting increased apoptotic cells with size and concentration-dependent exposures to bulk and TiO_2 nanoparticles. *In silico* analysis was done by docking tp53 protein (apoptotic factor) with TiO_2 nanoparticles as shown in Fig. 8 (C). The interaction was predicted through H-bonding with glutamic acid and arginine residues, having bond lengths of 3.10 Å, 2.96 Å and 3.07 Å, 3.14 Å and 2.80 Å, respectively, as mentioned in Table 2.

In silico predictions and experimental observations indicated a systematic relationship with oxidative stress, steatosis and apoptosis. The relationship was revealed through pathway analysis using STITCH[59] and analyzed by Cytoscape,[63] as shown in Fig. 10.

Discussion

This study depicts the biological *in vivo* cytotoxicity of industrially synthesized TiO_2 nanoparticles in an environmental

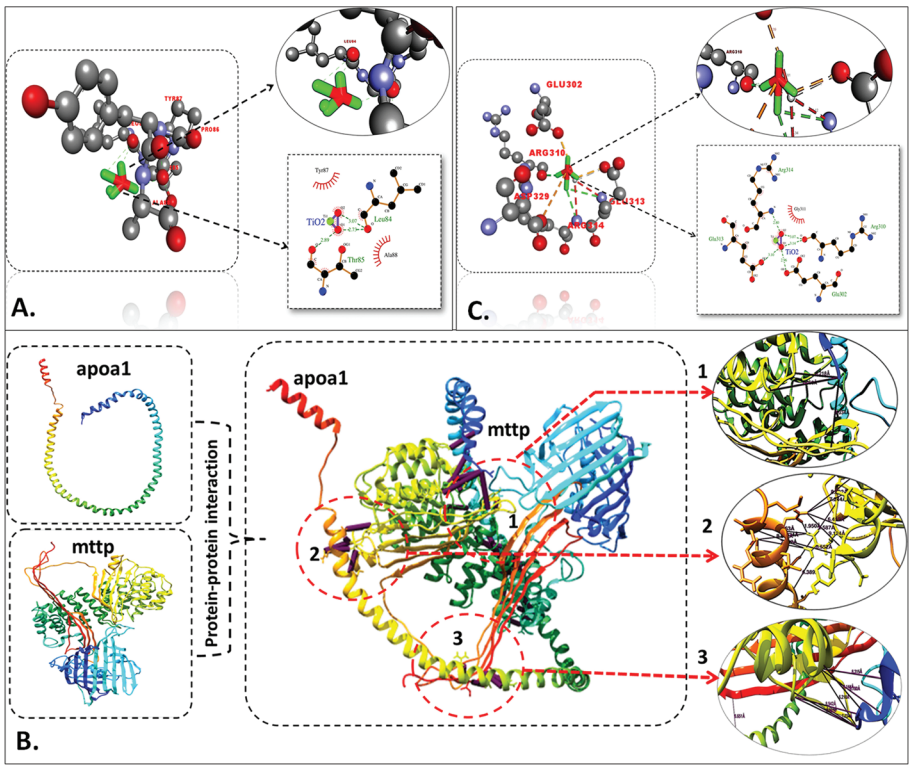

Fig. 8 Molecular docking analysis. (A) Interaction of apoa1a with TiO_2 nanoparticles showing interacting residues using LigPlot+ and Discovery Studio Visualizer. (B) Protein–protein interaction of MTTP and apoa1a proteins showing the site of interaction using Chimera. (C) Interaction of tp53 with TiO_2 nanoparticles, showing interacting residues using LigPlot+ and Discovery Studio Visualizer.

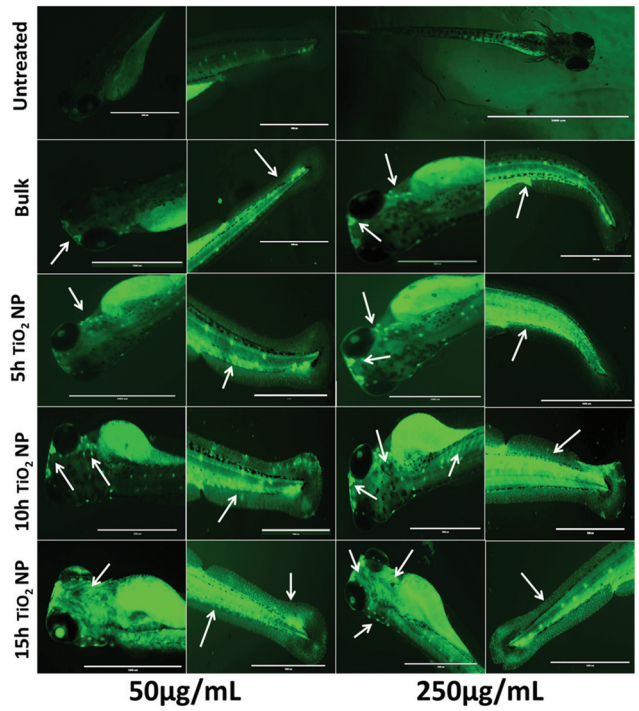

Fig. 9 Fluorescent images of zebrafish larvae stained with acridine orange (AO), treated with TiO_2 nanoparticles at concentrations of 50 µg mL^{-1} and 250 µg mL^{-1}, presenting apoptosis in the head and tail tissues. Arrows indicate the sites of apoptosis. Apoptosis was found to vary with the size and concentration of the nanoparticles.

aquatic system with mechanistic analysis using the embryonic zebrafish model. To explore the potential cytotoxicity, industrial synthesis of TiO_2 nanoparticles was imitated at the lab scale using the high energy ball milling technique (HEBM). Bulk TiO_2 was milled for 5 h, 10 h and 15 h in tungsten carbide container (WC) using WC balls at 10 : 1 BPR (ball to powder ratio) in toluene medium to prepare contamination free TiO_2 nanoparticles. During the synthesis, 300 rpm was used to avoid contamination. The HEBM technique has been reported in literature as one of the top-down approaches for the green synthesis of nanoparticles.[64] The high energy produced due to mechanical milling can be attributed to the reduction in the size of the materials to the nanoscale by grinding.[65] Many metal oxide nanoparticles have been reported to be synthesized using this method in last few years.[64] For cytotoxicity studies, nanoparticles milled for 5 h, 10 h and 15 h were collected and characterized by their physiochemical properties using known standard techniques. All the characterizations were performed in HF medium, which was used to rear zebrafish embryos in order to understand the physiochemical properties of TiO_2 nanoparticles in the respective biological media.

FESEM analysis showed a decrease in size with increased milling time. Hydrodynamic size determined by DLS supported the results of FESEM. However, the difference in size

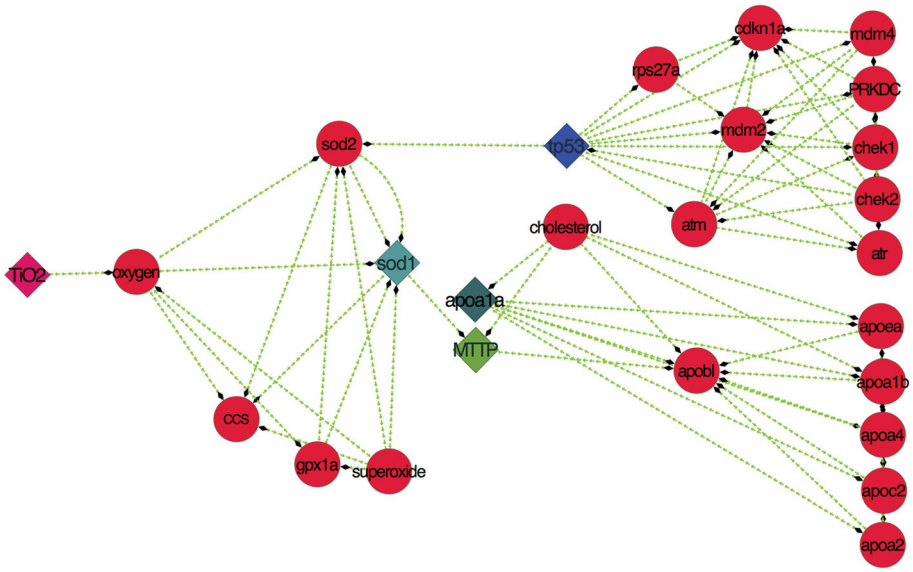

Fig. 10 Pathway showing the TiO_2 interaction mechanism involving sod1, apoa1a, MTTP and tp53 proteins derived from STITCH and analyzed using Cytoscape.

can be attributed to the attached water and salt molecules present in HF medium.[66] Zeta potential increased with milling time, which can be attributed to an increase in the core–shell intrinsic defects due to size reduction.[67] A blue shift in the surface plasmon resonance (SPR) peak was obtained in the UV-Vis spectra, with an increase in band gap energy, which can be attributed to the addition of a few molecular orbitals to the possible energy states of the particle with a reduction in size due to increased milling time,[68] leading to higher energy absorption. Characterization experiments confirmed the alteration of physiochemical property changes in TiO_2 nanoparticles with an increase in milling time in HEBM synthesis.

Previous reports have described the toxic effects of TiO_2 nanoparticles on the biological system using zebrafish as *in vivo* model.[20] Analysis of different toxicological parameters included the effect of nanoparticles on hatching, development, mortality and genetic effects of aquatic organisms (zebrafish), induced by their exposure due to accumulation in aquatic bodies.[69] In order to determine the cytotoxic effects of industrially synthesized TiO_2 nanoparticles on zebrafish embryos, different physiological parameters were checked by exposing them to groups of embryos. One of the important indicators of the quality of embryos and larvae of aquatic organisms is their hatchability.[70] To elucidate the effect of bulk and TiO_2 nanoparticles on the hatching of embryonic zebrafish, the hatching percentage was determined in a group of 20 embryos. Hatching analysis in the exposed embryos showed a significant difference with the size-dependent effects of bulk and TiO_2 nanoparticles exhibiting a reduction in hatching percentage accompanied by mortality rate enhancement. Zebrafish he1a, a zinc metalloprotease, has been recognized as the key factor for inducing the hatching of embryos.[58] Molecular analysis of TiO_2 nanoparticle interactions with hatching enzyme he1a showed hydrogen bonding with the asparagine amino acid residue. The hatching gland present in the chorion sac has been reported to digest the chorion for hatching through he1a enzymatic secretions.[58] It can be argued that the TiO_2 nanoparticles H-bonding interactions with he1a amino acid residues influence its enzymatic activity. This argument was clearly understandable from the pathway drawn with the help of STITCH and Cytoscape. The hatching rate reduction can therefore be attributed to the influential size-dependent interaction of exposed bulk and TiO_2 nanoparticles with he1a enzyme *via* the catalytic activity of an f2, which has been reported as a coagulation factor in the pathway.[71] Others factors like captopril and losartan were also found to be influential in the analysis. Moreover, the acuteness of hatching rate reduction with increase in milling time can be accredited to the residual stress that occurred in the nanoparticles due to the increased milling time. Previous studies have also reported the inhibition of hatching enzyme by nanoparticles interaction after being internalized through the chorion pore canals. Some reports have also described the cause of hatching rate abnormalities as due to the blocking of chorion pores on the accumulation of nanoparticles at the chorion surface, leading to a shortage of oxygen supply.[72,73] Zeta potential is regarded as a measurement of net charge in nanoparticles; from bulk to TiO_2 nanoparticles, it was found to increase with decreasing size, depicting a probable reason for higher attachment, accumulation and internalization across the chorion. It may also be argued to be a reason for greater blocking of pores leading to lower hatching rate. With reference to experimental and computational analysis, it can be concluded that the size-dependent accumulation of TiO_2 nanoparticles at the outer membrane of the embryonic chorion elicited the inhibition of hatching enzyme secreted from the hatching gland due to

structural changes induced by H-bond interaction with the asparagine residue. Inactivity of the hatching enzyme leads to failure of inner membrane digestion and ultimately reduction of the hatching rate.[58]

The TiO_2 nanoparticle cytotoxicity to embryonic zebrafish was further investigated with respect to the impacts on morphology and physiological processes. Acute morphological changes like edema, tail bending and abnormal yolk sac were observed in zebrafish exposed to 10 h and 15 h milled TiO_2 nanoparticles in comparison to bulk and 5 h milled TiO_2 nanoparticles. These symbolical toxicity effect features can be attributed to size and charge dependent accumulation, internalization, and interaction with outer covering skin and body fluids, which occurred due to the residual stress of milled TiO_2 nanoparticles. Similar features of toxicity were defined by Asharani *et al.*[74] and our previous study[75] in the case of the toxicity of silver nanoparticles. Further, in order to determine the cytotoxic effects of changes in the physiochemical properties of bulk and TiO_2 nanoparticles, uptake analysis was performed by analyzing the granularity change at the cellular level. The analysis showed significant size and concentration dependent uptake in a single cellular suspension of embryonic zebrafish, revealing the reason for the morphological and physiological changes due to exposure to bulk and TiO_2 nanoparticles.

Elicitation of physiological changes at the cellular level includes metabolic abnormalities in physiological processes like oxidative stress and lipid metabolism. Flow cytometric analysis of DCFDA fluorescence depicting ROS intensity in embryonic zebrafish cells exposed to bulk and TiO_2 nanoparticles showed the induction of enhanced ROS on exposure to bulk TiO_2 particles with a contradictory finding of ROS quenching in the case of 5 h, 10 h, and 15 h milled TiO_2 nanoparticles. The enhancement of ROS generation on exposure toTiO_2 nanoparticles has been reported previously.[76] This contradictory behavior of HEBM synthesized TiO_2 nanoparticles can be attributed to the generation of oxygen vacancies as a result of mechanical milling.[67] The milling of TiO_2 nanoparticles results in the exhibition of residual stress, creating oxygen vacancies. Nanotechnologists have previously reported the occurrence of oxygen vacancies in HEBM synthesized metal oxide nanoparticles as intrinsic defects.[67] These oxygen vacancies can be defined as the points in the crystal lattice where an electron is missing from the oxygen shell.[67,77] The increase in band gap energy with the decrease in size by increasing the milling time for TiO_2 nanoparticles confirmed the increase in oxygen vacancies. These oxygen vacancies react with a free electron of reactive oxygen species, acting as oxygen scavenger agents.[78] ROS has been recognized as a key element in the regulation of cellular physiological processes like hypoxia adaptors,[79] homeostasis maintenance,[80] *etc*. Influential ROS regulation can be attributed to the influential functionality of the sod1 gene on exposure to nanoparticles.[60] The analysis of *in silico* docking showed a direct interaction of TiO_2 nanoparticles with sod1 through H-bonding with phenylalanine and alanine residues. This interaction can be a probable cause of sod1 functionality, leading to oxidative stress abnormalities. The influential functionality of the sod1 gene has been previously reported in the response to different stimuli.[73,81,82]

The other probable aspect of cellular level metabolic abnormalities on exposure to TiO_2 nanoparticles is their effect on lipid metabolism, generally termed "steatosis".[83] An investigation of steatosis, *i.e.*, an accumulation of neutral lipid in embryonic zebrafish exposed to bulk and TiO_2 nanoparticles, was done. As shown in Fig. 7, enhanced accumulation was found in zebrafish larvae heads, notochords, and tail regions treated with bulk TiO_2 and nanoparticles in a size and concentration dependent manner. The neutral lipid metabolism alteration in zebrafish larval tissues can be attributed to the enhanced interaction of bulk and TiO_2 nanoparticles with the yolk syncytial layer due to increased zeta potential. During embryonic development, the yolk syncytial layer synthesizes apolipoproteins, which form very low-density lipid droplets (VLDL) and cytoplasmic LD from yolk lipids. These VLDLs and LDs then enter the circulatory system and deliver lipids to the tissue.[84] Computational molecular docking of apoa1a (apolipoprotein) with TiO_2 nanoparticles showed H-bonding with leucine and threonine residues, depicting the influence of TiO_2 nanoparticles on its activity. It can be interpreted with reference to these interactions that the production of VLDLs and LDs has been affected due to the molecular interference of nanoparticles. The transfer of these VLDLs and LDs are executed by microsomal triglyceride transfer protein (MTTP).[62,85] Protein–protein interaction molecular docking predictions of MTTP with apoa1a showed firm H-bond interactions depicting the functional effects of MTTP with respect to apoa1a. Lipid peroxidation has been reported to be induced by different nanoparticles.[86,87] Similarly, lipid alteration in the brain and gastrointestinal tissues of zebrafish by carbon based nanoparticles has been reported by Gorrochategui *et al.*[88] Based on these reports and our results, it can be estimated that the increase in neutral lipid accumulation in zebrafish larva on the treatment of bulk TiO_2 and nanoparticles is because of their size dependent molecular level interaction with lipid proteins.

Due to the toxicological effects, the outcome of these cellular abnormalities from exposure to industrially synthesized TiO_2 nanoparticles was deduced by cellular apoptosis determination. Apoptosis analysis was performed with acridine orange staining. Acridine orange is a nucleic acid specific dye that intercalates with DNA and emits a green color.[89] It permeates apoptotic cells and intercalates with DNA while normal cells are impermeable, thus indicating the site of apoptosis in zebrafish larvae. Increased quantities of apoptotic cells in the head and tail regions were observed with increasing concentration and exposure time of bulk TiO_2 and nanoparticles. The data also revealed the dependence of apoptosis on the increased milling time of bulk TiO_2 and nanoparticles. For cellular apoptosis induction in zebrafish, p53 has been reported to play a vital role during embryonic stages.[90,91] Molecular docking analysis of TiO_2 nanoparticles with tp53 showed

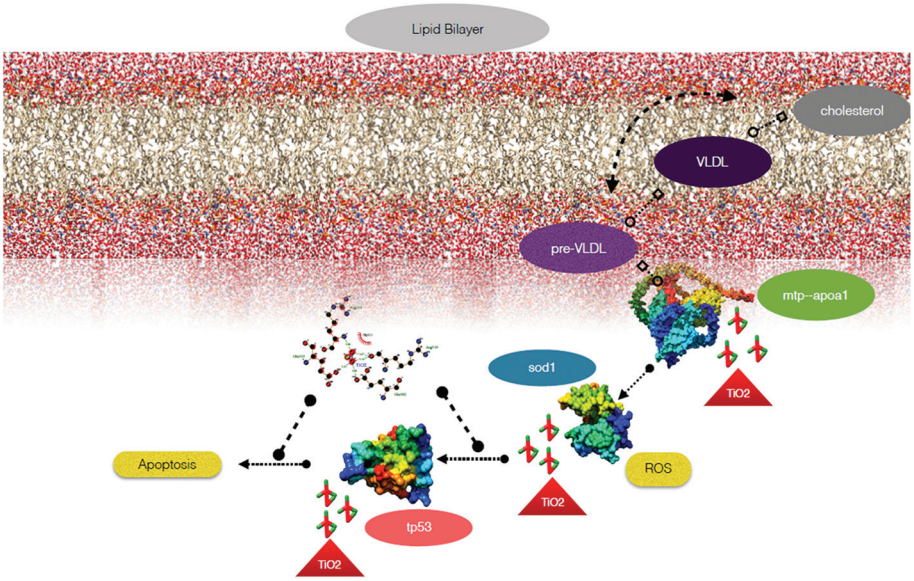

Fig. 11 Schematic representation of the effects of TiO_2 nanoparticles on oxidative stress, neutral lipid metabolism and apoptosis.

H-bonding with arginine and glutamic acid residues, indicating their influence. The effects of the significant differences in the size and charge of bulk TiO_2 and nanoparticles can be attributed to the elicited enzymatic activity of tp53 in inducing apoptosis.

From the experimental and computational results, it is assumed that there is a firm link among all the cytotoxic effects observed due to exposure to bulk and TiO_2 nanoparticles. To validate our assumption, the pathway was established through *in silico* data mining using STITCH and was represented by Cytoscape (Fig. 10). The pathway indicated that the altered physiochemical properties, such as size and zeta potential changes in TiO_2 nanoparticles due to mechanical milling of bulk TiO_2, induced differential cytotoxicity because of their discrepancy in oxygen vacancies. These oxygen vacancies influence the activity of sod1 protein *via* the activity of other proteins like sod2, gpx1a and cc, which in turn affect the apoptotic pathway by influencing tp53 protein function and many protein complexes. This protein complex played a role in enhancing the neutral lipid metabolism. Thus, the ROS quenching properties of synthesized TiO_2 nanoparticles can be the reason behind the induced apoptosis and lipid metabolism using sod1 as the central node of the pathway. The whole metabolic pathway is sketched in the schematic diagram in Fig. 11.

With the help of the experimental outcomes and computational analysis of the cellular physiological abnormalities induced by exposure to variable sized industrially synthesized TiO_2 nanoparticles, it can be deduced that accumulated bulk and TiO_2 nanoparticles induce cytotoxicity in zebrafish by altering their cellular physiological metabolic activities such as oxidative stress regulation and lipid metabolism at the molecular level by influencing the regulation of the responsible genes and proteins. Size-dependent abnormal oxidative stress due to quenching of ROS by nanoparticles affects different metabolic processes like neutral lipid metabolism, which in turn affects the whole metabolism, especially the induction of enhanced programmed cell death, leading to the size-dependent toxicity of TiO_2 nanoparticles.

Conclusion

This study has elucidated the impact of industrially synthesized bulk TiO_2 and nanoparticles on the aquatic biological system, using the zebrafish embryo model. TiO_2 nanoparticles prepared by the high-energy ball milling method (HEBM) were characterized for their physiochemical properties by DLS, XRD, FESEM, and UV-Vis spectroscopy. Characterisation confirmed the nano-sized nature of TiO_2 nanoparticles as well as determined the surface charge modification with respect to change in size. Determination of zeta potentials and flow cytometry analysis for nanoparticle uptake has illustrated the size and charge-dependent interaction followed by internalization of these nanoparticles in embryonic zebrafish. *In vivo* cytotoxicity analysis of bulk and TiO_2 nanoparticles in zebrafish embryos revealed their size and concentration-dependent effects on head, trunk and tail developmental deformities. TiO_2 nanoparticles were also found to enhance the scavenging of ROS and induction of apoptosis as well as neutral lipid alteration in accordance with their size and concentration variation through different molecular interactions. This study has described the size and charge-dependent nanotoxicity of industrially synthesized TiO_2 nanoparticles toward zebrafish cells. This is as a consequence of the exposure of the zebrafish to TiO_2 nanoparticles, which are subsequently internalised and influence the functionality of metabolic proteins, leading to abnormal cellular function. There is the potential for toxic

effects on the aquatic ecosystem, which can occur in the human system; this needs to be taken into account for the proper usage analysis. Moreover, this study has provided a detailed analysis of the toxicological outcomes of industrially synthesized TiO_2 nanoparticles, which will be helpful to determine the proper concentrations for the nanoparticle usage. It is therefore imperative that their application in day-to-day life and the quest for a more green method for producing TiO_2 nanoparticles with less cytotoxicity should be given special attention, considering their severity on the environment while embracing the potential benefits.

Conflicts of interest

There is no conflict of interest.

References

1 Y. K. Mishra and R. Adelung, *Mater. Today*, 2017, DOI: 10.1016/j.mattod.2017.11.003.
2 A. Nasajpour, S. Mandla, S. Shree, E. Mostafavi, R. Sharifi, A. Khalilpour, S. Saghazadeh, S. Hassan, M. J. Mitchell, J. Leijten, X. Hou, A. Moshaverinia, N. Annabi, R. Adelung, Y. K. Mishra, S. Shin, A. Tamayol and A. Khademhosseini, *Nano Lett.*, 2017, **17**(10), 6235–6240.
3 Y. K. Mishra, S. Kaps, A. Schuchardt, I. Paulowicz, X. Jin, D. Gedamu, S. Wille, O. Lupan and R. Adelung, *KONA Powder Part. J.*, 2014, **31**, 92–110.
4 A. Weir, P. Westerhoff, L. Fabricius, K. Hristovski and N. von Goetz, *Environ. Sci. Technol.*, 2012, **46**, 2242–2250.
5 R. R. Blakey and J. E. Hall, Titanium Dioxide, in *Pigment Handbook*, 1988, pp. 1–42.
6 W. Van Bussel, F. Kerkhof, T. Van Kessel, H. Lamers, D. Nous, H. Verdonk, B. Verhoeven, N. Boer and H. Toonen, *At. Spectrosc.*, 2010, **31**, 81–88.
7 M. A. Shaheed and F. H. Hussein, *J. Environ. Anal. Chem.*, 2014, **2**, 9–11.
8 M. M. Khan, S. A. Ansari, D. Pradhan, M. O. Ansari, D. H. Han, J. Lee and M. H. Cho, *J. Mater. Chem. A*, 2014, **2**, 637–644.
9 S. Kalathil, M. M. Khan, S. A. Ansari, J. Lee and M. H. Cho, *Nanoscale*, 2013, **5**, 6323.
10 M. M. Khan, S. A. Ansari, M. I. Amal, J. Lee and M. H. Cho, *Nanoscale*, 2013, **5**, 4427.
11 M. M. Khan, S. F. Adil and A. Al-Mayouf, *J. Saudi Chem. Soc.*, 2015, **19**, 462–464.
12 S. Mahata, S. S. Mahato, M. M. Nandi and B. Mondal, *Funct. Mater.*, 2012, **1461**, 225–228.
13 T. Santhoshkumar, A. A. Rahuman, C. Jayaseelan, G. Rajakumar, S. Marimuthu, A. V. Kirthi, K. Velayutham, J. Thomas, J. Venkatesan and S. K. Kim, *Asian Pac. J. Trop. Med.*, 2014, **7**, 968–976.
14 S. Indris, R. Amade, P. Heitjans, M. Finger, A. Haeger, D. Hesse, W. Grünert, A. Börger and K. D. Becker, *J. Phys. Chem. B*, 2005, **109**, 23274–23278.
15 T. Prasad Yadav, R. Manohar Yadav and D. Pratap Singh, *Nanosci. Nanotechnol.*, 2012, **2**, 22–48.
16 S. K. Verma, E. Jha, P. K. Panda, J. K. Das, A. Thirumurugan, M. Suar and S. Parashar, *Nanomedicine*, 2017, **13**, 43–68.
17 A. Kopp Alves, C. P. Bergmann and F. A. Berutti, *High-Energy Milling*, 2013, pp. 77–85.
18 H. J. Fecht, E. Hellstern, Z. Fu and W. L. Johnson, *Metall. Trans. A*, 1990, **21**, 2333–2337.
19 G. Mulas and F. Delogu, *High-Energy Ball Milling*, 2010.
20 N. B. Hartmann, S. Legros, F. Von der Kammer, T. Hofmann and A. Baun, *Aquat. Toxicol.*, 2012, **118–119**, 1–8.
21 G. Federici, B. J. Shaw and R. D. Handy, *Aquat. Toxicol.*, 2007, **84**, 415–430.
22 M.-S. Kim, K. M. Louis, J. a. Pedersen, R. J. Hamers, R. E. Peterson and W. Heideman, *Analyst*, 2014, **139**, 964–972.
23 Y. Guichard, J. Schmit, C. Darne, L. Gaté, M. Goutet, D. Rousset, O. Rastoix, R. Wrobel, O. Witschger, A. Martin, V. Fierro and S. Binet, *Ann. Occup. Hyg.*, 2012, **56**, 631–644.
24 J. Chen, X. Dong, J. Zhao and G. Tang, *J. Appl. Toxicol.*, 2009, **29**, 330–337.
25 A. Nel, *Science*, 2006, **311**, 622–627.
26 K. Saha, S. T. Kim, B. Yan, O. R. Miranda, F. S. Alfonso, D. Shlosman and V. M. Rotello, *Small*, 2013, **9**, 300–305.
27 R. E. Yanes, D. Tarn, A. A. Hwang, D. P. Ferris, S. P. Sherman, C. R. Thomas, J. Lu, A. D. Pyle, J. I. Zink and F. Tamanoi, *Small*, 2013, **9**, 697–704.
28 Y. Li, W. Zhang, J. Niu and Y. Chen, *ACS Nano*, 2012, **6**, 5164–5173.
29 S. K. Verma, E. Jha, B. Sahoo, P. K. Panda, A. Thirumurugan, S. K. S. Parashar and M. Suar, *RSC Adv.*, 2017, **7**, 40034–40045.
30 S. Hackenberg, G. Friehs, M. Kessler, K. Froelich, C. Ginzkey, C. Koehler, A. Scherzed, M. Burghartz and N. Kleinsasser, *J. Nanopart. Res.*, 2011, **268**, 264–268.
31 M. Premanathan, K. Karthikeyan, K. Jeyasubramanian and G. Manivannan, *Nanomedicine*, 2010, 1–9.
32 J. R. Gurr, A. S. S. Wang, C. H. Chen and K. Y. Jan, *Toxicology*, 2005, **213**, 66–73.
33 T. C. Long, N. Saleh, R. D. Tilton, G. V. Lowry and B. Veronesi, *Environ. Sci. Technol.*, 2006, **40**, 4346–4352.
34 L. Shang, K. Nienhaus and G. U. Nienhaus, *J. Nanobiotechnol.*, 2014, **12**, 5.
35 C. M. Sayes and D. B. Warheit, *Wiley Interdiscip. Rev.: Nanomed. Nanobiotechnol.*, 2009, **1**, 660–670.
36 J. M. Berg, A. Romoser, N. Banerjee, R. Zebda and C. M. Sayes, *Nanotoxicology*, 2009, **3**, 276–283.
37 M. Ghosh, A. Chakraborty and A. Mukherjee, *J. Appl. Toxicol.*, 2013, **33**, 1097–1110.
38 A. Jacobs, *Toxicol. Lett.*, 2009, **186**, 32–35.
39 A. Baun, N. B. Hartmann, K. Grieger and K. O. Kusk, *Ecotoxicology*, 2008, **17**, 387–395.
40 G. Xia, T. Liu, Z. Wang, Y. Hou, L. Dong, J. Zhu and J. Qi, *Artif. Cells, Nanomed., Biotechnol.*, 2015, 1–6.
41 J. S. Choi, R.-O. Kim, S. Yoon and W.-K. Kim, *PLoS One*, 2016, **11**, e0160763.

42 Y.-J. Wang, Z.-Z. He, Y.-W. Fang, Y. Xu, Y.-N. Chen, G.-Q. Wang, Y.-Q. Yang, Z. Yang and Y.-H. Li, *Int. J. Ophthalmol.*, 2014, **7**, 917–923.
43 O. Bar-Ilan, C. C. Chuang, D. J. Schwahn, S. Yang, S. Joshi, J. A. Pedersen, R. J. Hamers, R. E. Peterson and W. Heideman, *Environ. Sci. Technol.*, 2013, **47**, 4726–4733.
44 Z. Clemente, V. L. S. S. Castro, M. A. M. Moura, C. M. Jonsson and L. F. Fraceto, *Aquat. Toxicol.*, 2014, **147**, 129–139.
45 S. George, T. Xia, R. Rallo, Y. Zhao, Z. Ji, S. Lin, X. Wang, H. Zhang, B. France, D. Schoenfeld, R. Damoiseaux, R. Liu, S. Lin, K. A. Bradley, Y. Cohen and A. E. Nel, *ACS Nano*, 2011, **5**, 1805–1817.
46 J. Dharma, a. Pisal and C. Shelton, *Appl. Note*, 2009, 3–6.
47 M. Vaughan and R. Van Egmond, *ATLA, Altern. Lab. Anim.*, 2010, **38**, 231–238.
48 Q. Fang, X. Shi, L. Zhang, Q. Wang, X. Wang, Y. Guo and B. Zhou, *J. Hazard. Mater.*, 2015, **283**, 897–904.
49 J. Deng, L. Yu, C. Liu, K. Yu, X. Shi, L. W. Y. Yeung, P. K. S. Lam, R. S. S. Wu and B. Zhou, *Aquat. Toxicol.*, 2009, **93**, 29–36.
50 R. Thomsen and M. H. Christensen, *J. Med. Chem.*, 2006, **49**, 3315–3321.
51 O. Trott and A. Olson, *J. Comput. Chem.*, 2010, **31**, 455–461.
52 E. F. Pettersen, T. D. Goddard, C. C. Huang, G. S. Couch, D. M. Greenblatt, E. C. Meng and T. E. Ferrin, *J. Comput. Chem.*, 2004, **25**, 1605–1612.
53 A. C. Wallace, R. A. Laskowski and J. M. Thornton, *Protein Eng.*, 1995, **8**, 127–134.
54 G. Macindoe, L. Mavridis, V. Venkatraman, M. D. Devignes and D. W. Ritchie, *Nucleic Acids Res.*, 2010, **38**(Web Server issue), W445–W449.
55 X. Wei, G. Zhu, J. Fang and J. Chen, *Int. J. Photoenergy*, 2013, **2013**, 726872.
56 L. C. Wehmas, C. Anders, J. Chess, A. Punnoose, C. B. Pereira, J. A. Greenwood and R. L. Tanguay, *Toxicol. Rep.*, 2015, **2**, 702–715.
57 E. J. Zucker Massaro, K. M. Sanders, L. L. Degn and W. K. Boyes, *Cytometry, Part A*, 2010, **77**, 677–685.
58 K. Sano, K. Inohaya, M. Kawaguchi, N. Yoshizaki, I. Iuchi and S. Yasumasu, *FEBS J.*, 2008, **275**, 5934–5946.
59 D. Szklarczyk, A. Santos, C. Von Mering, L. J. Jensen, P. Bork and M. Kuhn, *Nucleic Acids Res.*, 2016, **44**, D380–D384.
60 C. F. Ken, C. T. Lin, J. F. Shaw and J. L. Wu, *Mar. Biotechnol.*, 2003, **5**, 167–173.
61 P. J. Babin, C. Thisse, M. Durliat, M. Andre, M. a. Akimenko and B. Thisse, *Proc. Natl. Acad. Sci. U. S. A.*, 1997, **94**, 8622–8627.
62 A. Schlegel and D. Y. R. Stainier, *Biochemistry*, 2006, **45**, 15179–15187.
63 M. Cline, M. Smoot, E. Cerami, A. Kuchinsky, N. Landys, C. Workman, R. Christmas, I. Avila-Campilo, M. Creech, B. Gross, K. Hanspers, R. Isserlin, R. Kelley, S. Killcoyne, S. Lotia, S. Maere, J. Morris, K. Ono, V. Pavlovic, A. Pico, A. Vailaya, P.-L. Wang, A. Adler, B. Conklin, L. Hood, M. Kuiper, C. Sander, I. Schmulevich, B. Schwikowski, G. Warner, T. Ideker and G. Bader, *Nat. Protoc.*, 2007, **2**, 2366–2382.
64 G. Mulas and F. Delogu, *High-Energy Ball Milling*, 2010, 45–62.
65 C. Suryanarayana, *Prog. Mater. Sci.*, 2001, **46**, 1–184.
66 Z. E. Allouni, M. R. Cimpan, P. J. Høl, T. Skodvin and N. R. Gjerdet, *Colloids Surf., B*, 2009, **68**, 83–87.
67 S. K. S. Parashar, B. S. Murty, S. Repp, S. Weber and E. Erdem, *J. Appl. Phys.*, 2012, **111**, 113712.
68 K. M. Reddy, S. V. Manorama and A. R. Reddy, *Mater. Chem. Phys.*, 2003, **78**, 239–245.
69 Y.-J. Dai, Y.-F. Jia, N. Chen, W.-P. Bian, Q.-K. Li, Y.-B. Ma, Y.-L. Chen and D.-S. Pei, *Environ. Toxicol. Chem.*, 2014, **33**, 11–17.
70 J. Zha and Z. Wang, *Agric., Ecosyst. Environ.*, 2005, **107**, 187–198.
71 K. Day, N. Krishnegowda and P. Jagadeeswaran, *Blood Cells, Mol., Dis.*, 2004, **32**, 191–198.
72 X. Zhao, S. Wang, Y. Wu, H. You and L. Lv, *Aquat. Toxicol.*, 2013, **136–137**, 49–59.
73 S. K. Verma, P. K. Panda, E. Jha, M. Suar and S. K. S. Parashar, *Sci. Rep.*, 2017, **7**, 13909.
74 P. V. Asharani, Y. Lian Wu, Z. Gong and S. Valiyaveettil, *Nanotechnology*, 2008, **19**, 255102.
75 S. K. Verma, E. Jha, P. Kumar Panda, A. Mishra, A. Thirumurugan, B. Das, S. Parashar and M. Suar, *Toxicol. Sci.*, 2018, **161**(1), 125–138.
76 M. Faria, J. M. Navas, A. M. V. M. Soares and C. Barata, *Sci. Total Environ.*, 2014, **470**, 379–389.
77 E. Erdem, P. Jakes, S. K. S. Parashar, K. Kiraz, M. Somer, A. Rüdiger and R.-A. Eichel, *J. Phys.: Condens. Matter*, 2010, **22**, 345901.
78 P. Trogadas, J. Parrondo and V. Ramani, *ACS Appl. Mater. Interfaces*, 2012, **4**, 5098–5102.
79 L. A. Sena and N. S. Chandel, *Mol. Cell*, 2012, **48**, 158–166.
80 G. Kroemer, G. Mariño and B. Levine, *Mol. Cell*, 2010, **40**, 280–293.
81 P. M. Craig, C. M. Wood and G. B. McClelland, *Am. J. Physiol. Regul. Integr. Comp. Physiol.*, 2007, **293**, R1882–R1892.
82 P. Kumari, P. K. Panda, E. Jha, K. Kumari, K. Nisha, M. A. Mallick and S. K. Verma, *Sci. Rep.*, 2017, **7**, 16284.
83 K. Minehira, S. G. Young, C. J. Villanueva, L. Yetukuri, M. Oresic, M. K. Hellerstein, R. V. Farese, J. D. Horton, F. Preitner, B. Thorens and L. Tappy, *J. Lipid Res.*, 2008, **49**, 2038–2044.
84 S. Martin and R. G. Parton, *Nat. Rev. Mol. Cell Biol.*, 2006, **7**, 373–378.
85 K. Stoletov, L. Fang, S. H. Choi, K. Hartvigsen, L. F. Hansen, C. Hall, J. Pattison, J. Juliano, E. R. Miller, F. Almazan, P. Crosier, J. L. Witztum, R. L. Klemke and Y. I. Miller, *Circ. Res.*, 2009, **104**, 952–960.

86 M. Li, J.-J. Yin, W. G. Wamer and Y. M. Lo, *J. Food Drug Anal.*, 2014, **22**, 76–85.
87 Y. Carrillo, C. Torres-Duarte, M. J. Oviedo, G. A. Hirata, A. Huerta-Saquero and R. Vazquez-Duhalt, *Appl. Ecol. Environ. Res.*, 2015, **13**, 709–723.
88 E. Gorrochategui, J. Li, N. J. Fullwood, G.-G. Ying, M. Tian, L. Cui, H. Shen, S. Lacorte, R. Tauler and F. L. Martin, *Mutagenesis*, 2017, **32**, 91–103.
89 P. Chapouton and L. Bally-Cuif, The Zebrafish: Cellular and Developmental Biology, in *Methods in Cell Biology*, 2004, http://www.sciencedirect.com/science/bookseries/0091679X/76.
90 N. Y. Storer and L. I. Zon, Zebrafish models of p53 functions, in *Cold Spring Harbor perspectives in biology*, 2010, vol. 2.
91 U. Langheinrich, E. Hennen, G. Stott and G. Vacun, *Curr. Biol.*, 2002, **12**, 2023–2028.